Combined experimental and multiphase computational fluid dynamics analysis of surface textured journal bearings in mixed regime of lubrication

Received: 20 March 2017 | Revised: 1 September 2017 | Accepted: 11 December 2017

DOI: 10.1002/ls.1414

RESEARCH ARTICLE - LS

WILEY

Combined experimental and multiphase computational fluid dynamics analysis of surface textured journal bearings in mixed regime of lubrication

N.J. Morris | H. Shahmohamadi | R. Rahmani | H. Rahnejat | C.P. Garner

Wolfson School of Mechanical, Electrical and Manufacturing Engineering, Loughborough University, Leicestershire, UK

Correspondence
R. Rahmani, Wolfson School of Mechanical, Electrical and Manufacturing Engineering, Loughborough University, Leicestershire, UK.
Email: r.rahmani@lboro.ac.uk

Funding information
Engineering and Physical Sciences Research Council; Lloyd's Register Foundation

Abstract

This paper investigates the effect of surface texturing in a partial pad journal bearing through a series of controlled experiments at operating conditions, promoting mixed or boundary regimes of lubrication. Improvements to load carrying capacity are observed under certain operating conditions. A comprehensive computational finite volume multiphase fluid dynamics analysis, including vapour transport equation and modified finite-size cavity Rayleigh-Plesset model, is used to study the effect of indented surface textures in the microscale contact domain and within the individual textures themselves. The results show improved conditions with a textured journal through promotion of micro-hydrodynamic effect, delaying the effect of lubricant rupture, thus extending the effective load bearing region. A very good agreement is obtained between measurements and predictions.

KEYWORDS

surface texturing, journal bearing, multiphase flow, cavitation, finite volume, CFD

Nomenclature: A, Apparent contact area; A_a, Asperity contact area; A_v, Area subjected to viscous friction; c, Bearing clearance; $E_{1,2}$, Young moduli of elasticity of journal and pad; E', Composite Young modulus of elasticity of contacting solids ($\frac{1}{E'} = \frac{1-\nu_1^2}{E_1} + \frac{1-\nu_2^2}{E_2}$); D, Journal diameter; e, Journal eccentricity; F_2, $F_{5/2}$, Statistical functions; f, Total friction; f_b, Boundary friction; f_{vis}, Viscous friction; f_v, Vapour mass fraction; g, Gravitational acceleration; h, Film thickness; h_0, Minimum film thickness; L, Bearing width or length; M_b, Torque due to boundary friction; M_{vis}, Torque due to viscous shear; p, Hydrodynamic pressure; p_{atm}, Atmospheric pressure; p_{sat}, Saturation/lubricant vaporisation pressure; R_j , Radius of journal; t, Time; u, Speed of lubricant entraining motion; v, Velocity of side-leakage flow along the bearing width; $\vec{V}$, Velocity vector; W, Contact reaction; W_a, Load carried by asperities; W_h, Hydrodynamic load carrying capacity; x, y, Lateral radial coordinates; z, Axial direction along the bearing width

Greek symbols: β, Average asperity tip radius; Γ, Diffusion coefficient; Δ, Sommerfeld number, $\frac{W}{u\eta L}\left(\frac{2c}{D}\right)^2$; Δ_{ij}, Kronecker delta; ε, Eccentricity ratio; η, Lubricant dynamic viscosity; θ, Circumferential direction in bearing; λ, Stribeck oil film parameter; μ, Pressure coefficient for boundary shear strength of asperities or coefficient of friction; ν, Poisson ratio; ξ, Number of asperity peaks per unit contact area; ρ, Lubricant density; σ, Standard deviation of surface roughness; ς, Pressure coefficient for boundary shear strength of asperities; τ, Shear stress; τ_0, Eyring shear stress; φ, Journal's attitude angle; $\phi_{1,2}$, Probability density function (PDF) of a surface height distribution; ϕ^*, Convolution of PDF of counterface surfaces; ω, Angular velocity

1 | INTRODUCTION

Surface texturing is progressively used as an approach to improve load carrying capacity of various tribological conjunctions, as well as mitigating frictional losses.[1,2] Dimples or other shallow cavities have been used to act as reservoirs of lubricant particularly in instances that lead to adverse operating conditions (eg, high load, low sliding speed, or poor lubricant availability). Such conditions inhibit the formation of a coherent film of lubricant, for example, during piston reversals. Research into surface texturing has been pursued vigorously because of the high share of piston frictional losses in all forms of crank-slider mechanisms (including in internal combustion engines). Some degree of success has been reported in various studies in palliation of friction and improvements to the output power[2-5] Furthermore, the underlying micro-hydrodynamic mechanism, causing pressure perturbations and enhanced lubricant film thickness, has been demonstrated by a number of detailed analytical and numerical analyses.[6-8] The same effects have also been noted for other tribological applications, particularly in the case of seals and thrust bearings, where the initial surface texturing work was conceived.[9-11]

The unfavourable operating conditions are not confined to pistons, seals, or thrust bearings but to all contact conjunctions that are subjected to stop-start, reciprocating, or inlet reversing conditions. These conditions result in mixed or boundary regimes of lubrication because of a diminishing lubricant entrainment into the contact. Use of surface coatings[5] or other forms of overlay[12] and lubricant rheology, particularly lubricant additives such as friction modifiers, have been commonplace in mitigating excessive boundary friction and thus the ensuing wear. In the case of engine conjunctions, the widely varying nature of transient regime of lubrication in different load bearing engine conjunctions means that an overall system solution to lubricant-surface combination cannot be realised. Thus, surface texturing as a localised approach may be regarded as a promising alternative.

Journal bearings are the most commonly used supporting element for rotating machinery, subjected to radial loading. In internal combustion engines, they are used as the main supporting elements for both the crankshaft and the camshaft. They are also used as the load transmitting elements for the connecting rod-crankshaft and the piston assemblies. Altogether, several journal bearings are used in any engine configuration, and they account for 25% of all the frictional losses of an engine, or equivalent to nearly 5% of the fuel consumption. In particular, the elliptic bore big-end bearings are subject to significant variations in the applied generated cyclic loading under a wide range of engine operating speeds.[12] These conditions are further exacerbated owing to the introduction of new technologies such as cylinder deactivation and intermittent stop-start engine operation in crawling traffic. While the growing take-up of these technologies heralds improvements in fuel efficiency and reduced emissions, recent studies have shown deteriorating frictional losses and other adverse tribological conditions, such as cavitation and transient thermal imbalance.[13,14] As the lubricant used is necessarily the same for all the engine conjunctions, there is only limiting opportunities for its rheological optimisation to suit all engine conjunctions. Thus, surface texturing and coatings are viewed as practical alternatives for improved contact conditions. The salient practical implications of multilayered overlays are adequately addressed in some studies.[12,15]

This paper focusses on the effect of surface texturing applied to the journal surface of a partial pad bearing. Lu and Khonsari[16] investigated the effect of dimple features in journal bearings, using several different texture dimensions. They showed that there was little accrued benefit under pure hydrodynamic regime of lubrication. The improvements were noted when running conditions pertained to a mixed regime of lubrication. Morris et al[17] also showed the same for a partial pad journal bearing, operating at low journal speeds, as did Galda et al.[6] Morris et al[17] observed that at higher journal speeds, resulting in hydrodynamic regime of lubrication, not only no significant benefit was noted with a textured journal but also increased side leakage, and thus oil loss was evident. This would be an issue of concern in terms of oil consumption, one which was also noted by Henry et al[11] for the case of thrust bearings. Therefore, a fundamental study of textured bearings using detailed numerical analysis is regarded as very timely. For the case of journal bearings, dimple textures have been the texture form of choice.[18-20] Therefore, dimple textures are used in the current study through use of indentation process.

When dealing with tribological problems, using Reynolds equation, where the roughness of the moving surface cannot be ignored or it incorporates special surface features, a transient form of Reynolds equation should be used. The differences emerge as a nonsmooth moving surface is shown to produce different effects compared to a nonsmooth fixed surface as shown in various studies.[21-26] Owing to this issue, the current study uses the full Navier-Stokes equations for 2-phase flow, including the effect of cavitation, which does not suffer from the usual assumptions made in deriving Reynolds equation. Therefore, inherently, the approach used includes both the spatial and temporal terms, such as the squeeze film effect and fluid inertia, as well as the usual viscous shear. In this approach, the problem is defined without the need for readjusting the coordinates or modifying any of the terms in the original set of equations. This certainly is not the case with

Reynolds equation. It is noteworthy that a study of pure squeeze of an impacting sphere on an oily plate performed by Al-Samieh and Rahnejat[27] with the coordinate system attached to the top layer of the lubricant to study the rapid squeeze caving phenomenon showed direct correspondence with the results obtained when the coordinate system was fixed to the stationary surface, while the moving surface fell under an equivalent gravitational effect (ie, squeeze effect). This is in fact known as the equivalence principle as an allusion to a relativistic framework. The results obtained by Al-Samieh and Rahnejat[27] agreed with the experimental work of Safa and Gohar.[28] Nevertheless, the use of Navier-Stokes approach in the current analysis alleviates the aforementioned usual assumptions of Reynolds approach.

In the current study, a multiphase flow through the journal-pad conjunction is expected as the lubricant film ruptures in the vicinity of the contact exit, preceding cavitation. It is also expected that with pressure perturbation occurring over the introduced microbearing areas (textures), the fall in generated pressure may induce localised vapour cavities in the scale of minutiae. To ensure continuity of multiphase flow, it is necessary to use a mass and momentum continuity analysis, using a combined solution of Navier-Stokes and vapour transport equations. This is the approach undertaken in the current analysis, which is in line with that described by Shahmohamadi et al,[14] who provided detailed experimental verification. The work by Shahmohamadi et al[14] is extended to the scale of minutiae and applied to the texture features on the surface of the journal, an approach not hitherto reported in literature.

2 | EXPERIMENTAL INVESTIGATION

2.1 | Experimental rig

The experimental rig shown in Figure 1 comprises a turned aluminium alloy journal, which is partially submerged in a reservoir of lubricant (sump). The journal is driven by an electric motor and a power pack at low speed (0-250 rpm), resulting in low speed of lubricant entrainment, thus promoting a mixed regime of lubrication. These conditions enable the study of enhanced lubrication when dimple textures are subsequently introduced on the journal surface. A 180° toughened acrylic bearing pad (bushing arc) conforms closely to the journal, forming a partial pad journal bearing arrangement. The pad is cut from an open cylinder. Weights are hung from the bearing pad to load the conjunction. A pointer is attached to the centre of the pad arc so that the attitude angle can be directly measured. The attitude angle is formed between the line of journal and the bearing pad centres and the vertically applied load. This angle is a direct measure of generated friction torque. The angle is read from a finely graduated scale attached to the test rig structure. Therefore, the attitude angle is used to infer the journal eccentricity and thus the generated friction. The properties of the lubricant selected for the experiment are listed in Table 1.

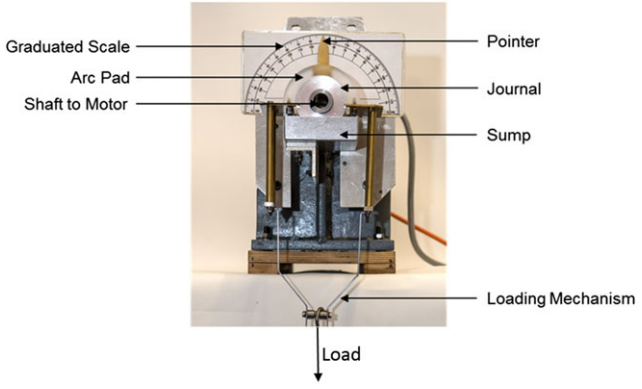

FIGURE 1 Experimental rig [Colour figure can be viewed at wileyonlinelibrary.com]

The lubricant used has the viscosity characteristics similar to those of formulated engine oils at start-up conditions (Table 1). The tests were performed at ambient temperature of 21°C ± 2°C.

The topography of the journal surface was measured using an infinite focus white light interferometer with a nominal vertical resolution of ±1 nm and a lateral sensitivity of 0.175 μm. The topography of the pad is measured using a stylus owing to its translucence. The stylus has a 90° conical angle and a tip radius of 2 μm. The geometrical forms of the journal and the pad were measured using a coordinate measurement machine with a measurement repeatability of ±1 μm. These are shown in Figure 2. The dimensions, out-of-roundness, and surface roughness of the journal and pad are provided in Table 2.

2.2 | Surface texturing

Two alternative journals are used. One is untextured, while the other has a textured surface with indented features (Figure 3). A survey of similar previous work drew on the reported experiences of others with regard to the density

TABLE 1 Lubricant data

Parameter	Value	Unit
Density at 288 K	894	kg m^{-3}
Kinematic viscosity at 295 K	512	mm^2 s^{-1}
Kinematic viscosity at 313 K	139	mm^2 s^{-1}
Kinematic viscosity at 373 K	14.3	mm^2 s^{-1}
Viscosity index	99	...
Sump volume	2.6×10^{-4}	m^3

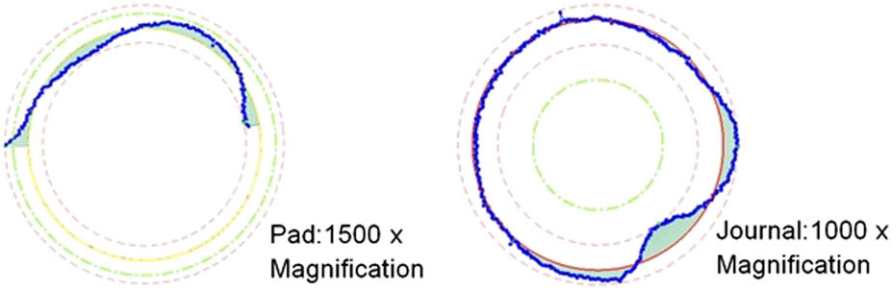

FIGURE 2 Measured geometrical form of the contacting surfaces [Colour figure can be viewed at wileyonlinelibrary.com]

TABLE 2 Test rig data

Parameter	Value	Unit
Journal diameter, D	65.6961	mm
Journal out-of-roundness	13.7	μm
Journal roughness ($R_{a,j}$, $R_{q,j}$)	0.035, 0.044	μm
Pad diameter	65.8576	mm
Pad out-of-roundness	7.5	μm
Pad roughness ($R_{a,p}$, $R_{q,p}$)	0.378, 0.526	μm
Material hardness (pad, journal)	(48HV30/10, 111HV60/10)	...

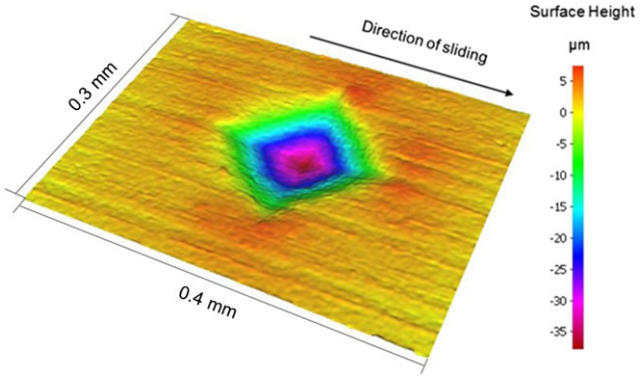

FIGURE 3 An individual surface texture taken by an infinite focus microscope [Colour figure can be viewed at wileyonlinelibrary.com]

distribution, depth, and diameter of indentations.[6,16,17] The contact conditions in the experimental study reside in the mixed regime of lubrication. A significant body of research has shown that under these conditions, low texture density produces the greatest reduction in friction.[18,29-32] Therefore, a low texture density is used for the journal surface.

The chosen values for the surface textures are shown in Table 3. The sizes of texture features and particularly their depth were also chosen in such a way that the size of the machining scars and marks on the shaft could be neglected in comparison. These values represent a compromise between the convenient production of surface textures using the readily available techniques such as indentation process and those suggested in open literature. A Vicker indenter was used to produce the surface textures and ensure a good repeatability for the

TABLE 3 Surface texture details

Parameter	Value	Unit
Centre-to-centre distance of textures	4.5	mm
Length × width	0.26 × 0.26	mm
Indentation depth	40	μm
Percentage textured area	0.33	%
Distribution pattern	Standard grid	...

indentation depth. A mesh of indented textures was fabricated onto the journal surface. Owing to the nature of the indention process, there was small variation in the size of dimples. However, this variation is quite small and can be neglected. Table 3 shows the average/typical size of the texture features, which is also used to create virtual textures in the numerical model.

Surface roughness measurement of the textured surface indicated that few protrusions or burrs were created during the surface texturing process. To remove any burrs, the journal was subjected to a running-in test procedure comprising 10 minutes' running period with a 2.2-kg load and at 1.5 rev s^{-1}. A separate pad was used during the running-in procedure, different to that used in the main tests. The surfaces then were examined using optical microscopy. It was observed that any burrs were completely removed during the running-in period.

2.3 | Experimental procedure

A repeatable test procedure was adopted to determine the effect of surface textures upon the tribological

performance of the partial pad journal bearing. The test rig was run at a given applied load for a range of journal speeds (36-180 rpm). The rotational speed of the journal was measured using a digital tachometer. The low speed of revolution results in an insufficient lubricant entrainment into the contact conjunction, thus promoting a mixed regime of lubrication. Under such conditions, the use of a textured journal is expected to promote microhydrodynamic effect, thus enhancing the lubricant film thickness and as a result palliating the effect of boundary generated friction. It should be noted that surface texturing is expected to reduce frictional losses under such circumstances. Therefore, the study reported here is instructive for such operating conditions and should not be regarded as optimal in a generic sense.

A steady speed was maintained for a set interval of time prior to each measurement. This was performed to avoid the complications arising from an initial squeeze film effect. After 4 measurements were taken at each chosen journal speed, the load was altered, and the same range of speed tests was undertaken. Owing to short duration of each test (of the order of a minute), the bulk lubricant temperature remains largely unaffected. Preliminary tests showed that the system reaches a stable state within a minute of testing. A short break was made between successive tests to ensure that the temperature of the lubricant sump was maintained at the recorded ambient temperature of 21°C ± 2°C. The bath of lubricant was maintained at the constant level of 20-mm immersion depth of the journal surface so that there would be a sufficient volume of lubricant to be entrained into the contact for an ideal fully flooded inlet.

At the beginning of each test, the bearing pad and the journal were separated and cleaned thoroughly so that any debris produced by a preceding test was removed. After subsequent reassembly, the rig was recalibrated, and a weight was hung from the pad ensuring, the orthogonal loading condition.

The attitude angle was measured using the pointer and the graduated scale. As the attitude angle varied slightly at a given applied load and speed, the average value of measured attitude angle is plotted under each test condition.

Each testing condition was repeated 4 times to ensure the repeatability of the presented outcomes.

Higher attitude angles are limited owing to the physical constraint of the loading mechanism, while the rotational speeds are limited by the splash of excess of lubricant from the oil sump.

2.4 | Experimental results

The experimental results for the untextured journal at various applied loads and speeds are shown in Figure 4.

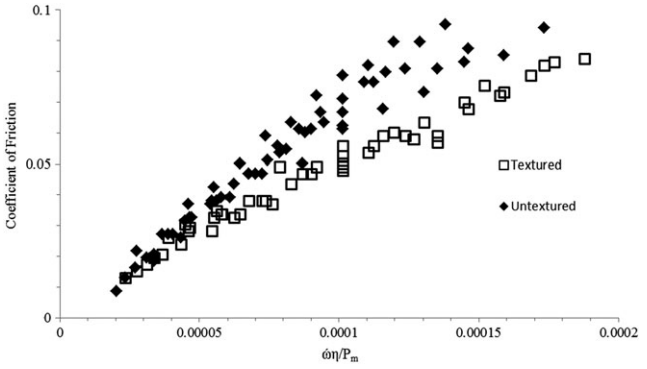

FIGURE 4 Variation of measured attitude angle with journal rotational speed for the case of an untextured journal

The results show that as the load decreases, the attitude angle increases as the ratio between the generated frictional torque and applied load alters.

The attitude angle can be related to the friction coefficient as $\mu \propto \tan \varphi$. The results shown in Figure 5 compare the textured and untextured results at different applied loads and journal speeds. At a load of 0.8 kg (Figure 5A), the boundary interactions are the least for all the tests performed. Under this condition, there is little difference between the coefficient of friction for the 2 cases (textured and untextured journals). As the load is increased in Figure 5B and 5C, the beneficial effect of surface textures becomes evident on the account of a reducing attitude angle at the higher journal speeds. At low speed conditions, the textured and untextured cases have very similar attitude angles, indicating that the textures have little benefit under the prescribed conditions. This is because at the very low sliding speeds, the contact is particularly starved of lubricant. These findings are in line with those of Lu and Khonsari[16] and Galda et al.[6]

The results in Figure 5D and 5E show the 2 clearest examples of benefits of surface texturing, with significant reductions in the recorded attitude angles (ie, proportional to the generated frictional torque).

Overall, the experimental results indicate that the introduced surface textures are beneficial under certain operating conditions. When the load is quite low, little difference is noted between the textured and untextured cases. When comparatively moderate loads are applied, the surface textures produce a beneficial effect. At higher loads and medium-to-low speeds, little advantage is accrued through use of a textured journal.

The benefit of surface texturing appears to be closely related to the prevailing regime of lubrication as it would be expected. All the experiments run in the mixed regime of lubrication. However, the extent of direct asperity interactions changes under different conditions. A numerical analysis of the experimental tests is required to further understand the salient underlying phenomena.

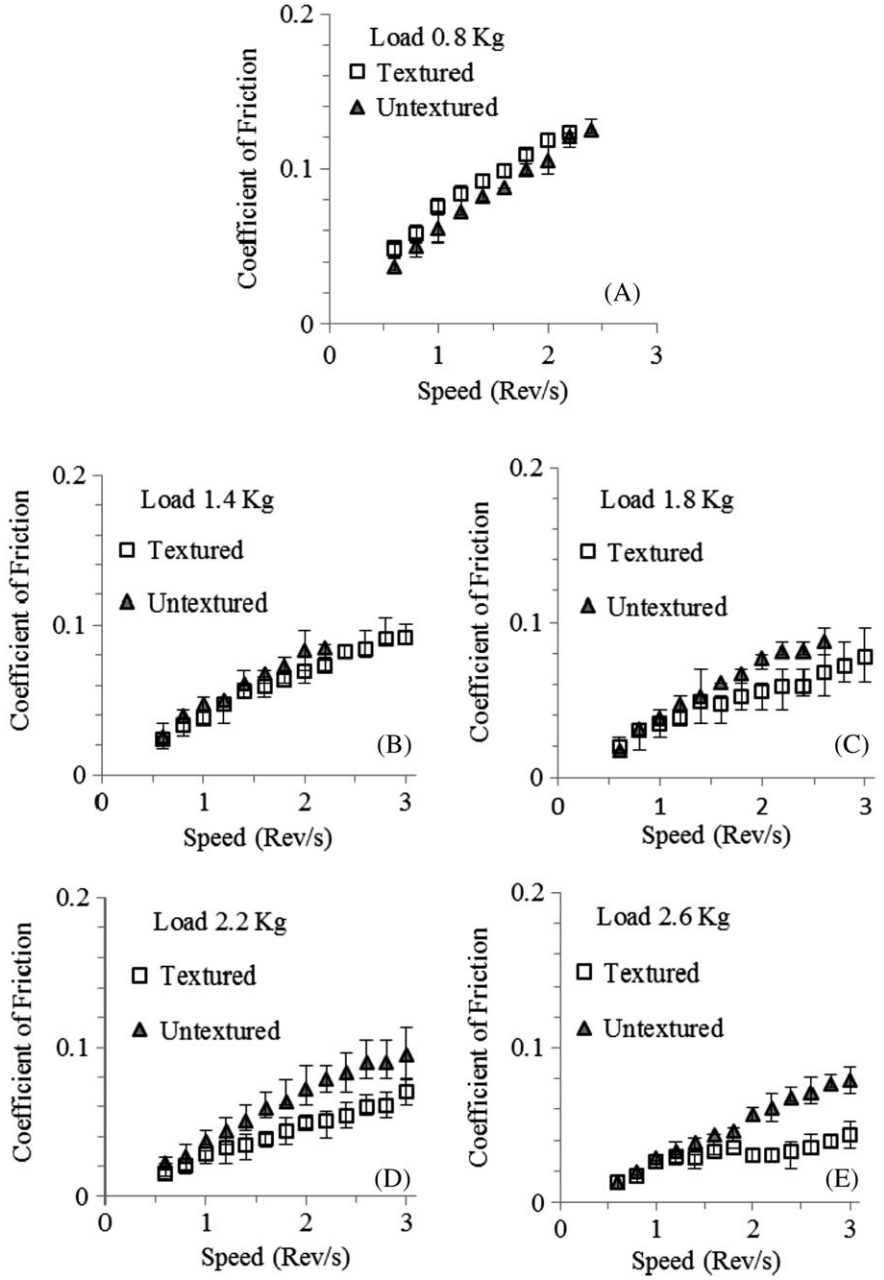

FIGURE 5 Comparison of coefficient of friction with changing speed for textured and untextured journals

3 | NUMERICAL MODEL

3.1 | Navier-Stokes equations

The governing equations for conservation of mass and momenta for each phase in the multiphase flow through the contact are[33]

$$\frac{D\rho_{\mathrm{l,v}}}{Dt} + \rho_{\mathrm{l,v}} \nabla \cdot \vec{V}_{\mathrm{l,v}} = 0, \tag{1}$$

$$\rho_{\mathrm{l,v}} \frac{D\vec{V}_{\mathrm{l,v}}}{Dt} = -\nabla p_{\mathrm{l,v}} + \nabla \cdot \left(\bar{\tau}_{ij}\right) + \vec{F}, \tag{2}$$

where the indices l and v denote the liquid and vapour phases, respectively. D/Dt is the covariant derivative operator, ρ is the lubricant density, p is the pressure, and $\bar{\tau}_{ij}$ is the viscous shear stress tensor. The body force field vector is $\vec{F}$. This is typically negligible for lubrication analysis, but left in the model for sake of generality. Furthermore, $\vec{V} = u\,\hat{i} + v\,\hat{j} + w\,\hat{k}$ is the velocity vector with u, v, and w being the components of the velocity in the 3 orthogonal Cartesian directions (x, y, and z). The viscous shear stress tensor is

$$\bar{\tau}_{ij} = \eta \left(\frac{\partial u_i}{\partial x_j} + \frac{\partial u_j}{\partial x_i} - \frac{2}{3} \Delta_{ij} \nabla \cdot \vec{V} \right), \tag{3}$$

where η is the effective lubricant dynamic viscosity and Δ_{ij} is the Kronecker delta.

3.2 | Cavitation model

To incorporate the cavitation effect, a model proposed by Singhal et al[34] was used, in which the growth of cavities is confined to a finite-size conjunction. This is particularly important in the small scale of indented textures. The transport equation for the vapour mass fraction is expressed as

$$\frac{\partial}{\partial t}(\rho f_v) + \vec{\nabla}\cdot\left(\rho f_v \vec{V}_v\right) = \vec{\nabla}\cdot\left(\Gamma \vec{\nabla} f_v\right) + R_e - R_c, \quad (4)$$

where Γ, f_v, and $\vec{V}_v$ denote diffusion coefficient, vapour mass fraction, and the vapour velocity vector, respectively.

The vapour generation and condensation rates were accounted for by using source terms, R_e and R_c, respectively. Following generalised Rayleigh-Plesset equations, Singhal et al[34] proposed the following expressions to take into account such phase change rates:

$$R_e = C_e \frac{V_{ch}}{S}\rho_l \rho_v \sqrt{\frac{2(p_{sat}-p)}{3\rho_l}}(1-f_v), \quad \text{for} \quad p \le p_{sat}. \quad (5)$$

$$R_c = C_c \frac{V_{ch}}{S}\rho_l \rho_v \sqrt{\frac{2(p-p_{sat})}{3\rho_l}} f_v, \quad \text{for} \quad p > p_{sat}. \quad (6)$$

In the relationships above, S represents the surface tension of the lubricant, while V_{ch} stands for the characteristic velocity, which can be considered as the local relative velocity between the liquid and vapour phases. It is assumed that no gasses are dissolved in the lubricant. Then, the saturation pressure, p_{sat}, can be considered to be equal to the bubble pressure in the cavitation zone at a given temperature. Finally, the empirical constants, C_e and C_c, specified by Singhal et al,[34] are 0.02 and 0.01, respectively.

3.3 | Asperity contact model for mixed and/or boundary regimes of lubrication

Direct interaction of solid surfaces occurs with a reducing journal speed. The interaction of asperities on the counterface surfaces result in mixed or boundary regimes of lubrication. Therefore, a portion of applied load is carried by the interacting asperities, while the remainder is supported by hydrodynamic reaction, thus

$$F = W_h + W_a, \quad (7)$$

where the hydrodynamic reaction force is obtained as

$$W_h = \iint p(\theta, z)\cos\theta r d\theta dz. \quad (8)$$

The load supported by asperities is a function of material properties and topographical properties of the counterfaces. It is important to determine the nature of topography of the counterface surfaces through measurement as reported in Section 2.1. Figure 6 shows that the measured topography of both the journal and the bearing pad conforms very well at 2.7σ from the mean roughness height as assumed by Greenwood and Tripp[35] and as for the majority of engineering surfaces. The area of interaction is shown in Figure 6A.

Then, the convoluted asperity height distribution or the probability density function of the 2 surfaces is described as

$$\phi^*(z) = \phi_1(z) * \phi_2(z). \quad (9)$$

The Greenwood and Tripp[35] statistical functions are defined as

$$F_n(\lambda) = \frac{1}{\sqrt{2\pi}}\int_\lambda^\infty (s-\lambda)^n \phi^*(s) ds, \quad (10)$$

where s is the intermediate integration variable. For asperity load carrying capacity of the counterfaces, $n = 5/2$ and for asperity contact area $n = 2$.

Therefore, the component of the load supported by the asperity tips in the direction opposite to the direction of

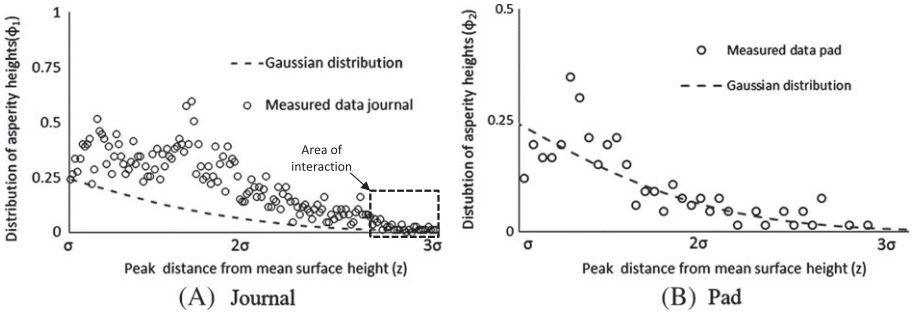

FIGURE 6 Measured probability distribution of asperity heights on the counterface surfaces

applied load can be expressed as[35]

$$W_a = \iint \frac{16\sqrt{2}}{15}\pi(\xi\beta\sigma)^2\sqrt{\frac{\sigma}{\beta}}E' r d\theta \cos\theta dz F_{5/2}(\lambda), \quad (11)$$

where E' is the composite effective modulus of elasticity of the contacting pairs, ξ is the unit area density of asperities, and β is the mean radius of curvature of tip of asperities. The statistical function $F_{5/2}(\lambda)$ is a function of the ratio of the film thickness to the combined standard deviation of the roughness of the contacting surfaces; ie, Stribeck oil film parameter $\lambda = h/\sigma$. For ease of computations, a polynomial-fit curve is used to approximate this statistical function, as follows[36]:

$$F_{5/2}(\lambda) = \begin{cases} -0.004\lambda^5 + 0.057\lambda^4 - 0.296\lambda^3 + 0.784\lambda^2 - 1.078\lambda + 0.617; & \text{for } \lambda \le \lambda_{cr} \\ 0; & \text{for } \lambda > \lambda_{cr} \end{cases}. \quad (12)$$

It is shown that the roughness parameter $\xi\beta\sigma$ is reasonably constant with a value in the range of 0.03 to 0.05 for engineering surfaces.[35-38] Furthermore, the ratio σ/β is normally in the range 10^{-4} to 10^{-2}.[27,30] The composite roughness parameter is obtained through $\sigma = \sqrt{R_{q,j}{}^2 + R_{q,p}{}^2}$ according to Gohar and Rahnejat.[38]

In the current study, the measured roughness parameter, $\xi\beta\sigma$, and average asperity slope, σ/β, provided mean values close to the upper limits of those typical ranges; ie, $\xi\beta\sigma = 0.05$ and $\sigma/\beta = 0.001$.

3.4 | Conjunctional friction

In the mixed regime of lubrication in journal bearings, the total frictional torque is obtained as

$$M_t = M_{vis} + M_b, \quad (13)$$

where the viscous torque, M_{vis}, is obtained through integration of the generated shear stress in the lubricant-surface interface as

$$M_{vis} = \iint \tau_v r^2 d\,\theta dz. \quad (14)$$

The frictional torque due to boundary friction can be described as follows:

$$M_b = f_b r \quad \text{where} \quad f_b = \tau_0 A_a + \varsigma W_a. \quad (15)$$

This model for friction (hence, torque) accounts for the direct asperity contact along with the non-Newtonian shear of pockets of lubricant entrapped between the asperities. The latter is accounted for by considering the limiting Eyring shear stress[39] for the lubricant used, which in this case is $\tau_0 = 2$ MPa.

Furthermore, the parameter ς, which is defined as the pressure coefficient for boundary shear strength of asperities on the softer counterface, is measured using an atomic force microscope in lateral force mode. To measure this parameter for the purpose of the current study, a similar procedure to that described by Buenviaje et al[40] and Styles et al[41] was followed.

The cumulative area of asperity tips, A_a, is found as[35]

$$A_a = \pi^2(\xi\beta\sigma)^2 A F_2(\lambda), \quad (16)$$

in which $F_2(\lambda)$ is a statistical function of Stribeck oil film ratio and a surface with Gaussian asperity distribution is given by[36]

$$F_2(\lambda) = \begin{cases} -0.0018\lambda^5 + 0.0281\lambda^4 - 0.1728\lambda^3 + 0.5258\lambda^2 - 0.8043\lambda + 0.5003; & \text{for } \lambda \le \lambda_{cr} \\ 0; & \text{for } \lambda > \lambda_{cr} \end{cases}, \quad (17)$$

where $\lambda_{cr} \approx 3$ is selected as the critical film ratio. Below this critical value, some degree of direct solid boundary interactions would be expected.

4 | BOUNDARY CONDITIONS AND SOLUTION PROCEDURE

Equations 1, 2, and 4 are solved through the use of finite volume method. For this purpose, a model is constructed using the ANSYS DesignModeler, which is subsequently spatially discretised using tetrahedral size–controlled elements. The entire flow domain is meshed using approximately 1 million tetrahedral cells. Each texture feature contains 260 finite volumes to ensure that the flow is accurately modelled. The current model assumes isothermal conditions.[42] A semi-implicit method for pressure-linked equations was used to couple the velocity field with pressure. In addition, a second-order upwind scheme is used for the discretisation of momenta and for minimising the discretisation errors.

With a constant applied load, the bearing eccentricity ratio depends on the pressure equilibrium over the journal surface. To compute eccentricity, the dynamic mesh method is used.[42]

An atmospheric pressure of 101 kPa is assumed at the outlet boundary, implying its exposure to the atmosphere, although Shen et al[43] have shown that cavitation pressures depend on machine running conditions and may be as low as 30 kPa for certain conditions. To take into account the cavitation effect in the tribological contacts, cavitation models and implementation algorithms such those proposed by Jakobsson and Floberg[44] and Olsson[45] or the Elrod cavitation algorithm[46] are commonly used. However, in the current study, the cavitation phenomenon is implemented through conjugate solution of the transport equation and the general Navier-Stokes equations. This removes the need for imposing any particular boundary condition(s) to specify either lubricant film rupture or reformation boundaries. This is a significant fundamental improvement upon the traditional cavitation implementation methods commonly used in the study of tribological conjunctions. Similar advantages can be obtained from alternative methods such as complementary-based models described by Woloszynski et al[47] and Giacopini et al,[48] who provided a 1D mass conserving method, based on a complementary algorithm and Reynolds equation. The algorithm is similar to the Elrod-Adams cavitation algorithm.

The bearing pad is stationary while the journal rotates. Both the solid boundaries are impermeable with lubricant slip assumed at these interfaces. The inlet and outlet pressures are set at the ambient pressure. Finally, the lateral boundaries of the bearing are open to atmosphere.

The analysis is advantageous as it allows for a more accurate description of the cavitation phenomenon. In addition, it allows for the variations of lubricant flow properties across the film. However, flow of lubricant through rough surfaces can also be significant. The average flow model developed by Patir and Cheng,[49] based on the original Reynolds equation, addresses this issue through introduction of flow factors. However, such a model has not been developed for a full set of Navier-Stokes equations. Therefore, it should be noted that the current analysis does not incorporate the roughness effect on the hydrodynamic flow of the lubricant.

5 | RESULTS AND DISCUSSION

5.1 | Model validation

Figures 7 and 8 show the predicted attitude angle for textured and untextured journal surfaces, as well as those measured under the same conditions and for 2 different applied loads. Note that an attitude angle of zero denotes the journal in static equilibrium (stationary) and subjected only to a normal vertical applied load. In all cases, the attitude angle is quite small, indicating a high eccentricity ratio, corresponding to mixed or boundary regimes of lubrication. This is due to the intentional low journal speeds chosen to promote such conditions, where surface texturing is likely to improve lubricant retention and mitigate undue boundary interactions. Good agreement is noted between the predictions and measurements. The numerical results show consistently slightly lower attitude angle for the textured journal, indicating lower contributions due to asperity interactions. The experimental results show the same trend with an increasing applied load.

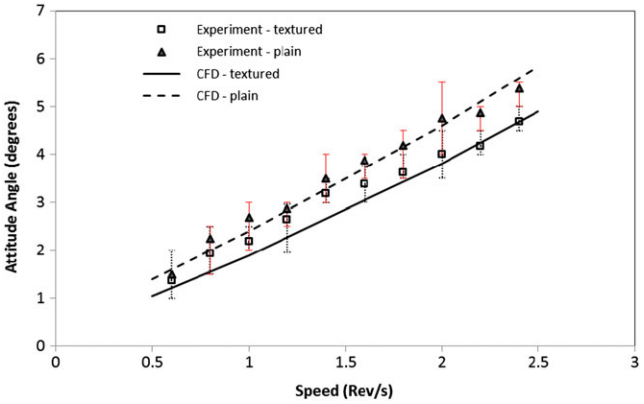

FIGURE 7 Changes in attitude angle over a range of speeds for a load of 1.4 kg (CFD and experimental results). CFD indicates computational fluid dynamics [Colour figure can be viewed at wileyonlinelibrary.com]

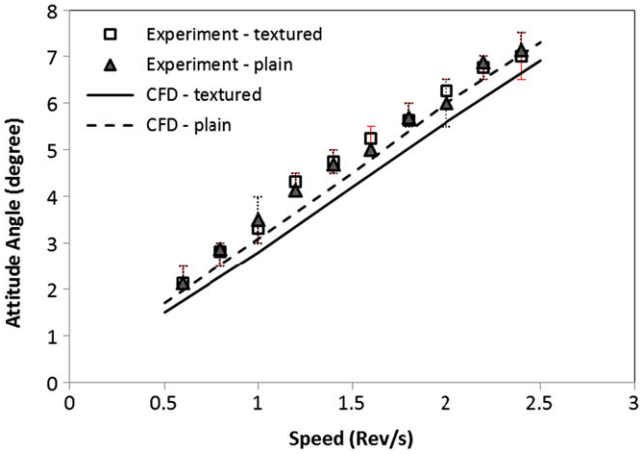

FIGURE 8 Changes in attitude angle over a range of speeds for a load of 0.8 kg (CFD and experimental results). CFD indicates computational fluid dynamics [Colour figure can be viewed at wileyonlinelibrary.com]

5.2 | Pressure distribution

With the validated numerical predictions, it is instructive to seek the underlying mechanism for the improved performance of the textured journal relative to the untextured case. Figure 9 shows the central pressure profiles of the generated hydrodynamic contact pressure distributions for the textured and untextured cases. These are coincident, as would be expected, with pressures generated in the first part of the arc of contact ($0 < \theta \leq \theta_c$, where θ_c is the lubricant film rupture point) with cavitation thereafter. There are pressure perturbations at the positions of the indented surface textures as indicated in the figure. Morris et al[8] noted the same for the case of a thin strip with a contacting face of a typical piston compression ring traversing a series of laser textured chevrons on a flat plate. They showed that the textured features retained a volume of lubricant, which caused pressure perturbation due to micro-hydrodynamic effect, enhancing the load carrying capacity of the contact, thus reducing the measured frictional torque. The results here indicate that the same phenomenon is responsible for improved conditions in the case of the textured journal.

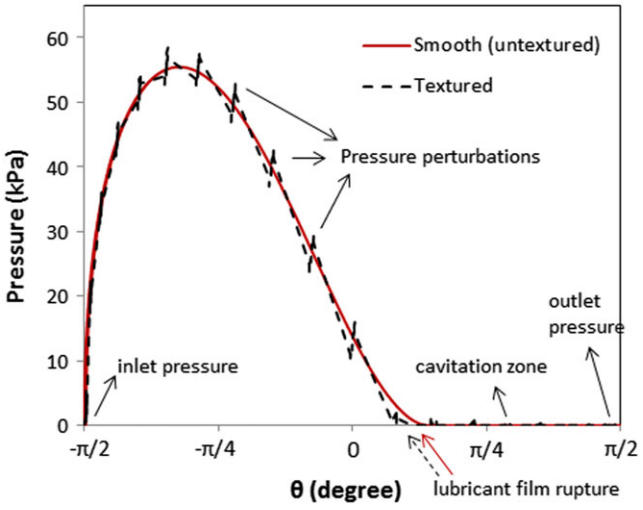

FIGURE 9 Pressure distribution in the centre plane for 1.4-kg load condition [Colour figure can be viewed at wileyonlinelibrary.com]

5.3 | State of flow

The state of flow through the contact and the extent of lubricated domain are good indications of the role of surface texturing. Figure 10 shows the predictions for multiphase flow through the contact, represented by the volume fraction of vapour content. A zero volume fraction represents regions of full liquid lubricant film (single-phase lubricant flow). It can be seen that the area of single-phase flow is extended further when a textured journal is used (Figure 10A), when compared with the untextured case (Figure 10B). The full lubricant film rupture boundary is at the onset of a finite vapour volume fraction (onset of vapour cavities). Therefore, the extent of full lubricant film region has increased with the use of texture features, which induce a micro-hydrodynamic effect through pressure perturbations (Figure 9) and thus enhance the contact load carrying capacity.

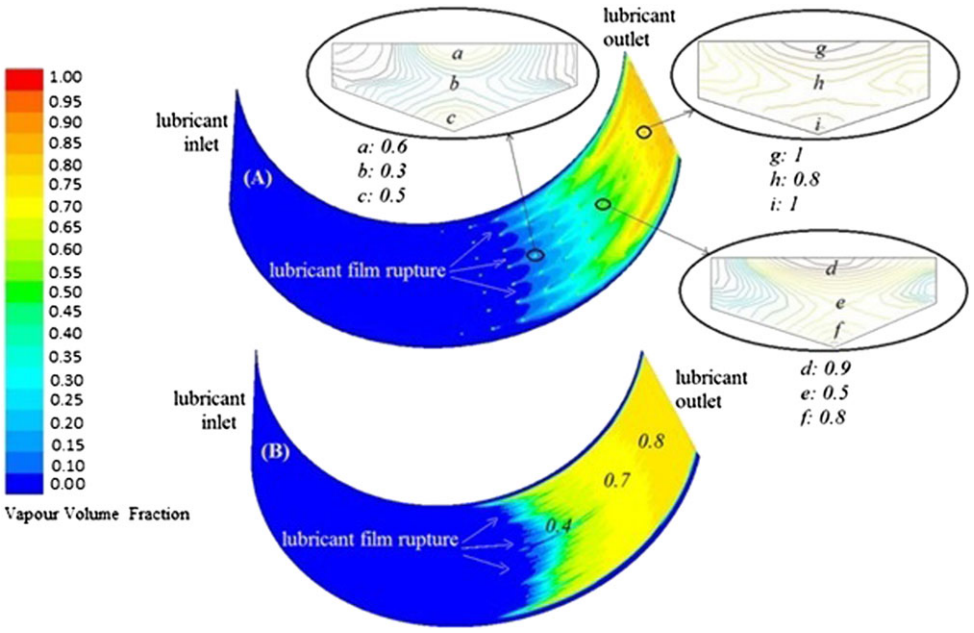

FIGURE 10 Contours of vapour volume fraction for (A) textured and (B) untextured journal bearing for a load of 1.4 kg [Colour figure can be viewed at wileyonlinelibrary.com]

Cavitation occurs at 2 distinct physical scales. At the larger scale (overall contact), there is the usual cavitation region beyond the lubricant film rupture boundary. In this region, and extending to the outlet of the contact, multiphase flow occurs with varying levels of vapour content. Cavitation also occurs at the local scale of an individual texture feature within the overall cavitation region. The multiphase flow dynamics within these textures is quite complex as can be seen in the various insets of Figure 10A. In all cases, there is some degree of swirl and counterflow, which yield a varying multiphase-layered content. This complex flow pattern gives rise to localised pressure perturbations even within the cavitation region, which is discernible in Figure 9 after the lubricant rupture boundary, prior to $\theta = \pi/2$ (contact outlet). The layered nature of the flow in texture features indicates pressure and density variations into the depth of film in all the regions of contact (ie, $\partial p/\partial z \neq 0$), which necessitates the combined solution of Navier-Stokes and vapour transport equations as highlighted in this paper, instead of the usual solutions using Reynolds equation.

Figure 11 shows the variations in load shared by asperities at different operational speeds and under various applied loads. As expected, at lower journal speeds, the asperity load share increases and reaches 11% of the total applied load, whereas at higher journal speeds, this contribution is merely 2% of the total load. This effect can be attributed to the build-up of hydrodynamic effect at higher speeds, generating a thicker lubricant film. The effect of the applied load is also shown in Figure 11. At higher loads, the asperities contribution is higher at all speeds particularly at lower ones. The effect of increasing the journal speed is to reduce the asperity load share, through formation a thicker film. In addition, the contribution of the asperities on carrying load seems to be largely insensitive to the application of the textures. The effect of texturing can best be observed at higher loads, where the mixed regime of lubrication is encountered, in line with expectation.

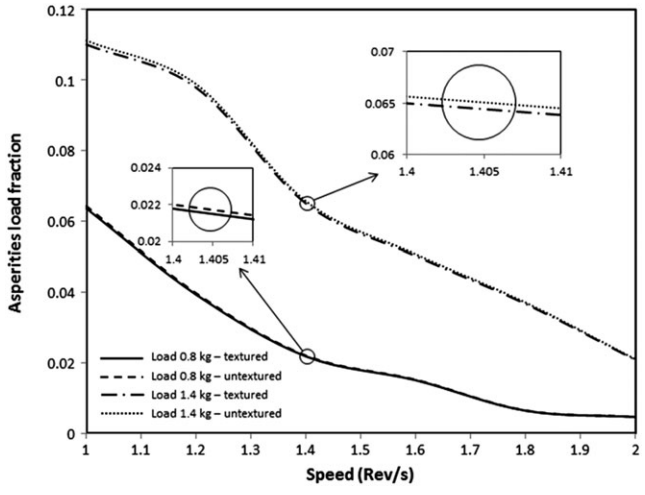

FIGURE 11 Fraction of applied load supported by the asperities at various journal speeds

It is shown that surface textures delay the onset of lubricant film rupture, thus extending the effective load carrying region of the conjunction. Furthermore, the textures cause micro-hydrodynamic pressure perturbation, which improve the local as well as overall load carrying capacity of the contact. Remarkably, their effect is reminiscent of the action of rough cartilage in natural endoarticular natural joints.[38] The flow of fluid within each individual texture is quite complex, comprising entrainment, reverse, and counterflows, but overall demonstrates a layered nature, clearly with density variations heralding some form of discretisation. This would obviously require further in-depth analysis, particularly with very shallow features to ascertain when the continuum nature of such microflows may be breached.

6 | CONCLUSIONS

Effect of texturing of journal surface in a partial pad journal bearing is investigated through a series of experiments at operating conditions, which promote mixed or boundary regimes of lubrication. Improvements to load carrying capacity are observed under certain conditions. A comprehensive computational finite volume multiphase fluid dynamics analysis, including vapour transport equation and modified finite-size cavity Rayleigh-Plesset void fraction model, is used to study the effect of indented surface textures on the microscale of the contact domain as well as the scale of the individual textures themselves. More than 1 million tetrahedral elements are used in the analysis.

The presented analysis is isothermal. In most relevant applications, generated temperatures can lead to more complex thermal cavitating flows, which in turn may need the inclusion of compressible liberated gas behaviour. These issues constitute the future direction of research into the optimisation of texture geometries.

It is also shown that any gain in tribological performance is marginal and confined to certain envisaged operating conditions such as stop-start and under conditions that promote mixed regime of lubrication. However, this marginal gain, if attained, over a number of bearing conjunctions in, for example, a typical engine and over a large number of vehicles, can have significant accrued economic and environmental impacts. More comprehensive analysis would be required, including texture geometry, density, and distribution as well as a broader range of operating conditions prior to practical applications under

the broad engine operating conditions. The work of Tala-Ighil et al[18] demonstrates the complex behaviour of surface texturing in the hydrodynamic regime of lubrication. In hydrodynamic conditions, increased texture area can lead to side leakage and oil loss.

ACKNOWLEDGEMENTS

The authors would like to express their gratitude to the financial support provided by Lloyd's Register Foundation (LRF), which is extended through the International Institute for Cavitation Research (ICR: http://www.cavitation-institute.org/) to this project. The authors would also like to acknowledge the UK Engineering and Physical Sciences Research Council (EPSRC) for the Encyclopaedic Program Grant (www.encycloapedic.org) as some of their research findings are used in this research.

ORCID

R. Rahmani http://orcid.org/0000-0002-6084-8842

REFERENCES

1. Etsion I. State of the art in laser surface texturing. *Trans. ASME, J. Tribology*. 2005;125:248-253.
2. Etsion, I., "Surface Texturing for In-cylinder Friction Reduction", New Delhi (India): Woodhead Publishing Ltd, 2010.
3. Rahnejat H, Balakrishnan S, King PD, Howell-Smith S. In-cylinder friction reduction using a surface finish optimization technique. *Proc. IMechE, Part D: J. Automobile Engineering*. 2006;220:1309-1318.
4. Ronen A, Etsion I, Kligernman Y. Friction-reducing surface texturing in reciprocating automotive components. *Tribology Transactions*. 2001;44:359-366.
5. Howell-Smith S, Rahnejat H, King PD, Dowson D. Reducing in-cylinder parasitic losses through surface modification and coating. *Proc. IMechE, Part D: J. Automobile Engineering*. 2014;228:391-402.
6. Galda L, Pawlus P, Sep J. Dimples shape and distribution effect on characteristics of Stribeck curve. *Tribology International*. 2009;42:1505-1512.
7. Balakrishnan S, Howell-Smith S, Rahnejat H. Investigation of reciprocating conformal contact of piston skirt-to-surface modified cylinder liner in high performance engines. *Proc. IMechE, Part C: J. Mechanical Engineering Science*. 2005;219:1235-1247.
8. Morris N, Leighton M, De la Cruz M, Rahmani R, Rahnejat H, Howell-Smith S. Combined numerical and experimental investigation of the micro-hydrodynamics of chevron-based textured patterns influencing conjunctional friction of sliding contacts. *Proc. IMechE, Part J: J. Engineering Tribology*. 2015;229:316-335.
9. Brizmer V, Kligerman Y, Etsion I. A laser surface textured parallel thrust bearing. *Tribology Transactions*. 2003;46:397-403.
10. Wang X, Kato K, Adachi K, Aizawa K. The effect of laser texturing of SiC surface on the critical load for the transition of water lubrication mode from hydrodynamic to mixed. *Tribology International*. 2001;34:703-711.
11. Henry Y, Bouyer J, Fillon M. An experimental analysis of hydrodynamic contribution of textured thrust bearings during steady-state operation: a comparison with untextured parallel surface configuration. *Proc. IMechE, Part J: J. Engineering Tribology*. 2015;229:362-375.
12. Balakrishnan S, McMinn C, Baker CE, Rahnejat H. Fundamentals of crank and camshaft support journal bearings. In: *Tribology and Dynamics of Engine and Powertrain*. Cambridge, UK: Woodhead Publishing; 2010.
13. Mohammadpour M, Rahmani R, Rahnejat H. Effect of cylinder deactivation on the tribo-dynamics and acoustic emission of overlay big end bearings. *Proc. IMechE, Part K: J. Multi-body Dynamics*. 2014;228:138-151.
14. Shahmohamadi H, Rahmani R, Rahnejat H, Garner CP, Dowson D. Big end bearing losses with thermal cavitation flow under cylinder deactivation. *Tribology Letters*. 2015;57:1-17.
15. Hoag, K.L., "Engine bearing design", Chapter 11 in: *Vehicular Engine Design,* 2006, pp. 125-141.
16. Lu X, Khonsari MM. An experimental investigation of dimple effect on the Stribeck curve of journal bearings. *Tribology Letters*. 2007;27:169-176.
17. Morris, N., Rahmani, R. and Rahnejat, H., "Tribology of partial pad journal bearings with textured surfaces", 3rd European Conference on Tribology, ECOTRIB, 2011, pp. 645-650
18. Tala-Ighil N, Fillon M, Maspeyrot P. Effect of textured area on the performances of a hydrodynamic journal bearing. *Tribology International*. 2011;44(3):211-219.
19. Cupillard S, Glavatskih S, Cervantes MJ. Computational fluid dynamics analysis of a journal bearing with surface texturing. *Proc. IMechE Vol. 222 Part J: J. Engineering Tribology*. 2008;222(2):97-107.
20. Brizmer V, Kligerman Y. A laser surface textured journal bearing. *Trans ASME, J. Triboogy*. 2012;134(3):031702-031711.
21. Buscaglia G, Ciuperca I, Jai M. Homogenization of the transient Reynolds equation. *Asymptotic Analysis*. 2002;32(2):131-152.
22. Bayada G, Ciuperca I, Jai M. Homogenized elliptic equations and variational inequalities with oscillating parameters. Application to the study of thin flow behavior with rough surfaces. *Nonlinear Analysis*. 2006;7:950-966.
23. Almqvist A, Essel EK, Persson E-E, Wall P. Homogenization of the unstationary incompressible Reynolds equation. *Tribology International*. 2007;40:1344-1350.
24. Shen D, Salant R. An unsteady mixed soft EHL model, with application to a rotary lip seal. *Tribology International*. 2007;40:646-651.
25. Gherca A, Fatu A, Hajjam M, Maspeyrot P. Influence of surface geometry on the hydrodynamic performances of parallel bearings in transient flow condition. *Tribology Transactions*. 2013;56:953-967.
26. Gherca A, Fatu A, Hajjam M, Maspeyrot P. Influence of surface texturing on the hydrodynamic behavior of a thrust bearing

operating in steady-state and transient lubrication regime. *Tribology International*. 2016;102(4):305-318.

27. Al-Samieh MF, Rahnejat H. Physics of lubricated impact of a sphere on a plate in a narrow continuum to gaps of molecular dimensions. *J. Phys., D: Applied Physics*. 2002;35(18):2311
28. Safa MMA, Gohar R. Pressure distribution under a ball impacting a thin lubricant layer. *Trans. ASME, J. Tribology*. 1986;108:372-376.
29. Kovalchenko A, Ajayi O, Erdemir A, Fenske G. Friction and wear behavior of laser textured surface under lubricated initial point contact. *Wear*. 2011;271(9):1719-1725.
30. Kovalchenko A, Ajayi O, Erdemir A, Fenske G, Etsion I. The effect of laser texturing of steel surfaces and speed-load parameters on the transition of lubrication regime from boundary to hydrodynamic. *Tribology Transactions*. 2004;47(2):299-307.
31. Wang X, Kato K, Adachi K, Aizawa K. The effect of laser texturing of SiC surface on the critical load for the transition of water lubrication mode from hydrodynamic to mixed. *Tribology International*. 2001;34(10):703-711.
32. Podgornik B, Vilhena LM, Sedlaček M, Rek Z, Žun I. Effectiveness and design of surface texturing for different lubrication regimes. *Meccanica*. 2012;47(7):1613-1622.
33. White FM. *Viscous Fluid Flow*. 2nd ed. McGraw-Hill; 1991.
34. Singhal A.K., Li H.Y., Athavale M.M., and Jiang Y., "Mathematical basis and validation of the full cavitation model", ASME FEDSM'01 Conference, New Orleans, Louisiana, 2001
35. Greenwood JA, Tripp JH. The contact of two nominally flat rough surfaces. *Proc IMechEJ. Mechanical Engineering Science*. 1970–1971;185:625-634.
36. Teodorescu M, Balakrishnan S, Rahnejat H. Integrated tribological analysis within a multi-physics approach to system dynamics. *Tribol. Interface Eng. Ser.* 2005;48:725-737.
37. Greenwood JA, Williamson BP. Contact of nominally flat surfaces. *Proc. Roy. Soc. Lond. Ser. A*. 1966;295:300-319.
38. Gohar R, Rahnejat H. *Fundamentals of tribology*. London: Imperial College Press; 2008.
39. Eyring H. Viscosity, plasticity and diffusion as examples of reaction rates. *J. Chem. Phys.* 1926;4:283-291.
40. Buenviaje CK, Ge S-R, Rafaillovich MH, Overney RM. Atomic force microscopy calibration methods for lateral force, elasticity, and viscosity. *Mater. Res. Soc. Symp. Proc.* 1998;522:187-192.
41. Styles G, Rahmani R, Rahnejat H, Fitzsimons B. In-cycle and life-time friction transience in piston ring-liner conjunction under mixed regime of lubrication. *Int. J. Engine Research.* 2014;15:862-876.
42. Manninen M, Taivassalo V, Kallio S. *On the Mixture Model for Multiphase Flow*", VTT Publications 288. Technical Research Centre of Finland; 1996.
43. Shen C, Khonsari MM. On the magnitude of cavitation pressure of steady-state lubrication. *Tribology Letters*. 2013;51:
44. Jakobsson B, Floberg L. *The Finite Journal Bearing Considering Vaporization*. Gothenburg: Trans. of Chalmers University of Tech; 1957.
45. Olsson KO. *Cavitation in Dynamically Loaded Bearings*. Gothenburg: Trans. of Chalmers University of Technology; 1965.
46. Elrod HG. A cavitation algorithm. *Trans. ASME, J. Lubr. Technol*. 1981;103:350-35s.
47. Woloszynski T, Podsiadlo P, Stachowiak GW. Efficient solution to the cavitation problem in hydrodynamic lubrication. *Tribology Letters*. 2015;58:
48. Giacopini M, Fowell MT, Dini D, Strozzi A. A mass-conserving complementarity formulation to study lubricant films in the presence of cavitation. *J. Tribol*. 2010;132:
49. Patir N, Cheng HS. An average flow model for determining effects of three-dimensional roughness on partial hydrodynamic lubrication. *J. Tribology.* 1978;100(1):12-17.

How to cite this article: Morris NJ, Shahmohamadi H, Rahmani R, Rahnejat H, Garner CP. Combined experimental and multiphase computational fluid dynamics analysis of surface textured journal bearings in mixed regime of lubrication. *Lubrication Science*. 2018;30:161–173. https://doi.org/10.1002/ls.1414